Earth and Planetary Science Letters 319-320 (2012) 259–268

Contents lists available at SciVerse ScienceDirect

Earth and Planetary Science Letters

journal homepage: www.elsevier.com/locate/epsl

Cape Verde hotspot from the upper crust to the top of the lower mantle

Lev Vinnik [a,*], Graça Silveira [b,c], Sergei Kiselev [a], Veronique Farra [d], Michael Weber [e,f], Eleonore Stutzmann [d]

[a] Institute of physics of the Earth, B. Grouzinskaya 10, 123995 Moscow, Russian Federation
[b] Instituto Dom Luiz, Campo Grande, Edificio C8, 1749-016 Lisboa, Portugal
[c] Area Cientifica de Fisica, Instituto Superior de Engenharia de Lisboa, 1959-007 Lisboa, Portugal
[d] Institut de Physique du Globe de Paris, PRES Sorbonne Paris Cité, CNRS UMR 7154, 1 rue Jussieu, 75005 Paris, France
[e] Deutsches GeoForschungsZentrum, Potsdam, Germany
[f] Institut fuer Erd- und Umweltwissenschaften, Universitaet Potsdam, Potsdam, Germany

ARTICLE INFO

Article history:
Received 26 May 2011
Received in revised form 8 November 2011
Accepted 14 December 2011
Available online xxxx

Editor: L. Stixrude

Keywords:
hotspot
plume
crust
upper mantle
mantle transition zone
receiver function

ABSTRACT

We investigate the crust, upper mantle and mantle transition zone of the Cape Verde hotspot by using seismic P and S receiver functions from several tens of local seismograph stations. We find a strong discontinuity at a depth of ~10 km underlain by a ~15-km thick layer with a high (~1.9) Vp/Vs velocity ratio. We interpret this discontinuity and the underlying layer as the fossil Moho, inherited from the pre-hotspot era, and the plume-related magmatic underplate. Our uppermost-mantle models are very different from those previously obtained for this region: our S velocity is much lower and there are no indications of low densities. Contrary to previously published arguments for the standard transition zone thickness our data indicate that this thickness under the Cape Verde islands is up to ~30 km less than in the ambient mantle. This reduction is a combined effect of a depression of the 410-km discontinuity and an uplift of the 660-km discontinuity. The uplift is in contrast to laboratory data and some seismic data on a negligible dependence of depth of the 660-km discontinuity on temperature in hotspots. A large negative pressure–temperature slope which is suggested by our data implies that the 660-km discontinuity may resist passage of the plume.

Our data reveal beneath the islands a reduction of S velocity of a few percent between 470-km and 510-km depths. The low velocity layer in the upper transition zone under the Cape Verde archipelago is very similar to that previously found under the Azores and a few other hotspots. In the literature there are reports on a regional 520-km discontinuity, the impedance of which is too large to be explained by the known phase transitions. Our observations suggest that the 520-km discontinuity may present the base of the low-velocity layer in the transition zone.

1. Introduction

Hotspots present a controversial topic, especially from geophysical perspective. Many experts follow Morgan (1971) in the idea that hotspots are generated by plumes ascending from the boundary layer at the base of the mantle. Courtillot et al. (2003) suggested that there are three distinct types of hotspots: primary or 'Morganian', of a very deep origin (1); secondary, from the transition zone (2); and 'tertiary' or 'Andersonian', of a superficial origin (3). Interpretations of seismic data for the deep mantle either claim evidence of deep roots of many hotspots (e.g., Montelli et al., 2006) or put it in doubt (Ritsema and Allen, 2003). Seismic anomalies that are found in the mantle transition zone beneath hotspots (e.g., Deuss, 2007) are refuted in other studies (Tauzin et al., 2008), and there are other arguments in favor of shallow origins of hotspots (e.g., Anderson, 2010; Doglioni et al., 2005) A reason for the contradictions is, partly, in a highly variable quality and resolution of seismic data. In many global studies the only robust mantle anomalies beneath hotspots are low S velocities at depths less than ~200 km, but they lack continuity at larger depths (Ritsema and Allen, 2003; Silveira et al., 2006). The best chances for resolving the details are provided by arrays of seismic stations sampling the Earth beneath hotspots in different directions and at a close range, but such arrays are few.

In this paper we use a local array of seismograph stations to investigate architecture of the Cape Verde hotspot in the Atlantic (Fig. 1). The Cape Verde archipelago consists of 9 main islands (Fig. 1) in the south-western part of the Cape Verde Rise, the underwater swell 1200 km in diameter. The swell is ~2 km high over the surrounding ocean floor 125–150 Myrs old. It is associated with elevated surface heat flow (Courtney and White, 1986) and a geoid anomaly of +8 m (Monnereau and Casenave, 2000). The Cape Verde Rise formed in the early Miocene, around 22 Myrs. The onset of volcanism on eastern islands (Sal, Boavista and Maio) is in the middle Miocene (~15 Myrs). The volcanism continued in Pliocene but on a reduced scale. The volcanism on the north-western (Santo Antão, Sao Vicente, Sao Nicolau) and south-western (Brava, Fogo, Santiago) islands is younger (~6 Myrs),

* Corresponding author.
E-mail address: vinnik@ifz.ru (L. Vinnik).

0012-821X/$ – see front matter © 2011 Elsevier B.V. All rights reserved.
doi:10.1016/j.epsl.2011.12.017

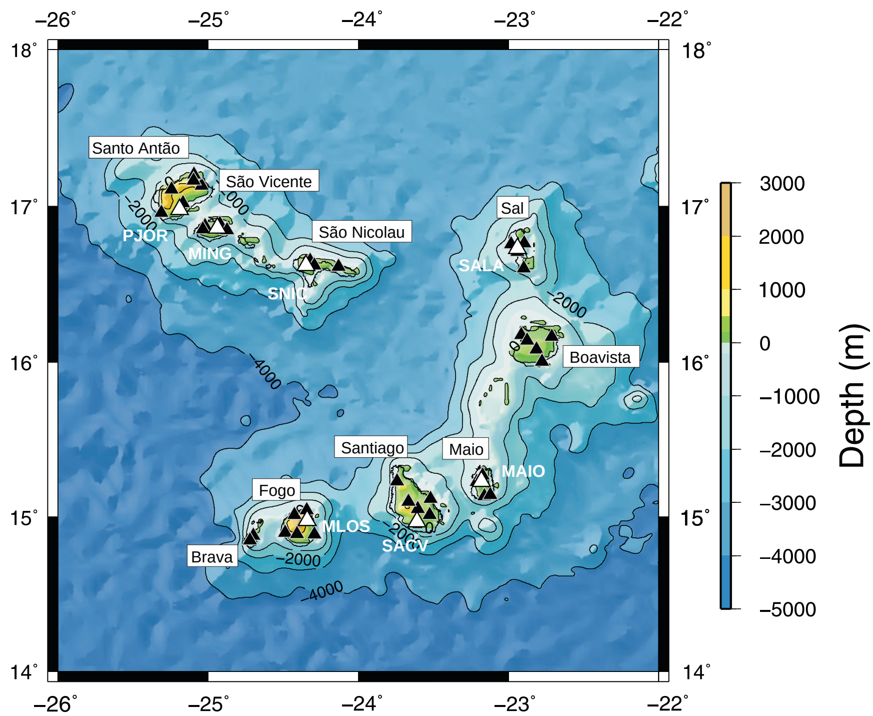

Fig. 1. Map of the region. The stations deployed in 2009 are shown by filled triangles. SACV is the station of the Global Seismograph Network. The other stations shown by open triangles were deployed in 2002–2004 (Helffrich et al., 2010). (For interpretation of the references to color in this figure legend, the reader is referred to the web version of this article.)

and it continues until today (Holm et al., 2008). The Cape Verde hotspot is almost stationary (Gripp and Gordon, 2002).

Seismic data are, generally, in favor of deep origins of the Cape Verde swell. Davaille et al. (2005) relate it to a large-scale velocity anomaly in the lower mantle but note the lack of reliable images of the mantle between 400-km and 1000-km depths. Seismic tomography data suggest that the origin of the Cape Verde plume is near the core–mantle boundary (Montelli et al., 2006). Thermochemical modeling of seismic and gravity data (Forte et al., 2010) reveals beneath the Cape Verde islands a deep-seated large-scale hot upwelling.

Seismic data for the crust, upper mantle and transition zone in the Cape Verde region are controversial. A hotspot swell can be explained by a thermal reheating of the lithosphere and/or magmatic underplating and/or dynamic support of upwelling asthenosphere. A joint analysis of gravity (free air anomalies) and seismic data (wide angle seismic reflections) suggests that the first two reasons are unlikely for the Cape Verde archipelago (Pim et al., 2008). The results of our work disagree with this solution.

Lodge and Helffrich (2006) inferred from receiver functions that the S velocity in the uppermost mantle is very high (4.8 km/s) and the mantle root of the swell is depleted. Thermal anomalies in the transition zone are expressed by anomalous depth separations between the 410-km and 660-km discontinuities. Helffrich et al. (2010) state that beneath the Cape Verde islands this separation is normal, with implication of 'Andersonian' origin of this hotspot. The results of our work are very different, practically the opposite.

We use recordings of station SACV of the Global Seismographic Network (GSN) on the island of Santiago and of two temporary networks. One network of ~40 stations was deployed in 2009 for 9 months. The recordings of several stations on each island were stacked to reduce noise and then treated as recordings of one station on this island. The 2nd network of several stations was deployed for 2 years from 2002 to 2004 (Lodge and Helffrich, 2006). Data of good quality were obtained at 6 stations: MLOS, MAIO, SALA, SNIC, MING and PJOR (Fig. 1). We will discuss the data with reference to the station codes (for the 2nd network) or to the island name (for the first network). Like in geological studies (Holm et al., 2008) we divide the islands into eastern (Sal, Boavista, Maio), north-western (Santo Antão, Sao Vicente, Sao Nicolau) and south-western (Brava, Fogo, Santiago) groups. We investigate the subsurface structure with P and S receiver function techniques, and, in this respect, this study is similar to the recent study of the Azores hotspot (Silveira et al., 2010). In Section 2 we present results of application of P receiver function techniques. These data illuminate the structure of the transition zone. P receiver functions are then complemented by S receiver functions (Section 3). Simultaneous inversion of the P and S receiver functions provides data on velocity profiles in the crust and upper mantle to a depth of ~300 km (Section 4). Finally, in Section 5 we summarize and discuss our findings.

2. P receiver functions

P receiver functions (PRFs) are used in our work for two purposes. First, we are interested in the structure of the mantle transition zone. Second, PRFs in the time interval from −5 s to 35 s are inverted simultaneously with SRFs for the crust and upper mantle velocity models. We use the LQ coordinate system (Vinnik, 1977) where the L axis corresponds to the principal direction of the P wave particle motion in the wave propagation plane and Q is perpendicular to L in the same plane. The records were low-pass filtered with a corner period of 6 s. To remove the effect of seismic source, the Q component of each seismic event is deconvolved by the L component, and the deconvolved Q components are stacked with move-out time corrections. The corrections are calculated for several assumed depths of conversion from 0 to 1000 km. The reference slowness for stacking, as in other similar studies, is 6.4 s/°. Seismic events used in the calculations of PRFs are distributed in a broad distance and azimuth range (Fig. 2).

PRFs in Fig. 3 consist mainly of Ps converted phases and multiple reflections. The Ps converted phases from transition-zone discontinuities and reverberations may arrive in the same time window but with a different slowness. The slowness of the Ps converted phases is less

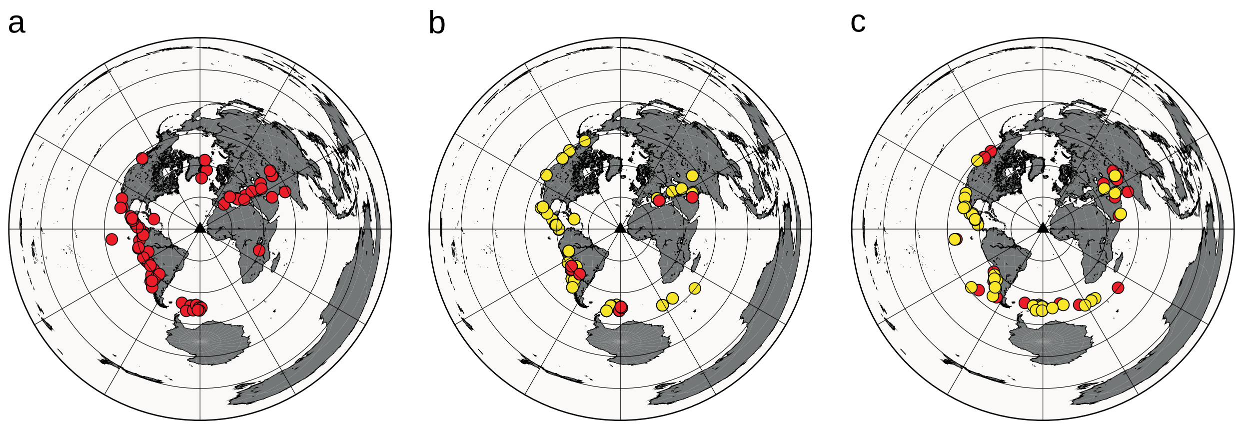

Fig. 2. Epicenters of seismic events used for constructing PRFs and SRFs: a) PRFs, station SACV; b) PRFs, stations deployed in 2009 (red) and 2002–2004 (yellow); c) SRFs, station SACV (yellow) and stations deployed in 2002–2004 (red). (For interpretation of the references to color in this figure legend, the reader is referred to the web version of this article.)

than of the P wave at the same epicentral distance, whilst that of the multiples is larger. To identify the converted phases with confidence, we follow Chevrot et al. (1999) and present in Fig. 1S (Supplementary material) the results of slant stacking, where the move-out corrections are calculated as product of the differential slowness (difference of the trial slowness relative to the P wave) and the differential distance (separation in epicentral distance between the seismic event and the average distance of the group of events). In this stack the largest amplitudes of the converted Ps phases and the multiples should be observed at a negative and positive differential slowness, respectively. All phases that are discussed in this Section are with a negative slowness. All stacks contain a large Ps phase from a crustal boundary at a time near 2 s. To judge on the region in the upper mantle sampled by PRFs, we show piercing points of the converted phases at 410-km and 660-km depths (Fig. 4).

The stack in Fig. 3a is obtained for the receiver functions from 9 events at ~15 stations on the north-western islands. Beyond the crustal phase, the stack contains a large pulse of negative polarity at a time of 53.6 s. It is labeled “M” because its waveform resembles the capital letter M. The piercing points (Fig. 4a) surround the north-western islands.

The stack of 20 PRFs for station PJOR (Fig. 3b) contains Ps phases from both 410-km and 660-km discontinuities at a time of 47.2 s and 70.6 s. The difference in time of the two phases (23.4 s) is reasonably close to the standard value (23.9 s) of IASP91 model with implication that the discontinuities in the transition zone sampled by PJOR are located close to their standard depths, but these arrivals are delayed by 3.2 s and 2.7 s with respect to the standard times of IASP91 model (Kennett and Engdahl, 1991). The times of IASP91 for P410s and P660s phases are very close to the average observational values in the

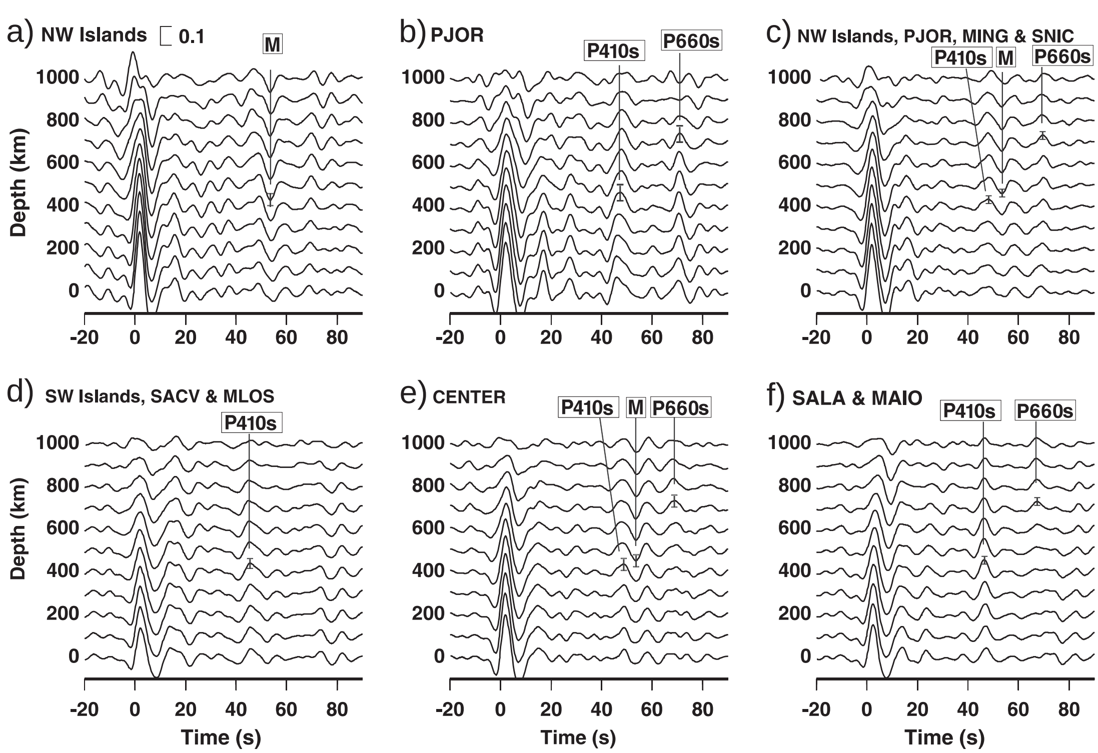

Fig. 3. Stacked PRFs from a) stations deployed in 2009 on the north-western islands, b) station PJOR, c) all stations on the north-western islands, d) all stations on the south-western islands, e) all stations on the north-western islands, southern events and all stations on the south-western islands, northern events, and f) stations SALA and MAIO. Each trace is obtained by migration to the depth shown on the left-hand side; Ps phases from the transition zone are marked by $\pm 2\sigma$ error bars on the traces for the migration depths of 400 km (P410s), 500 km (M) and 700 km (P660s).

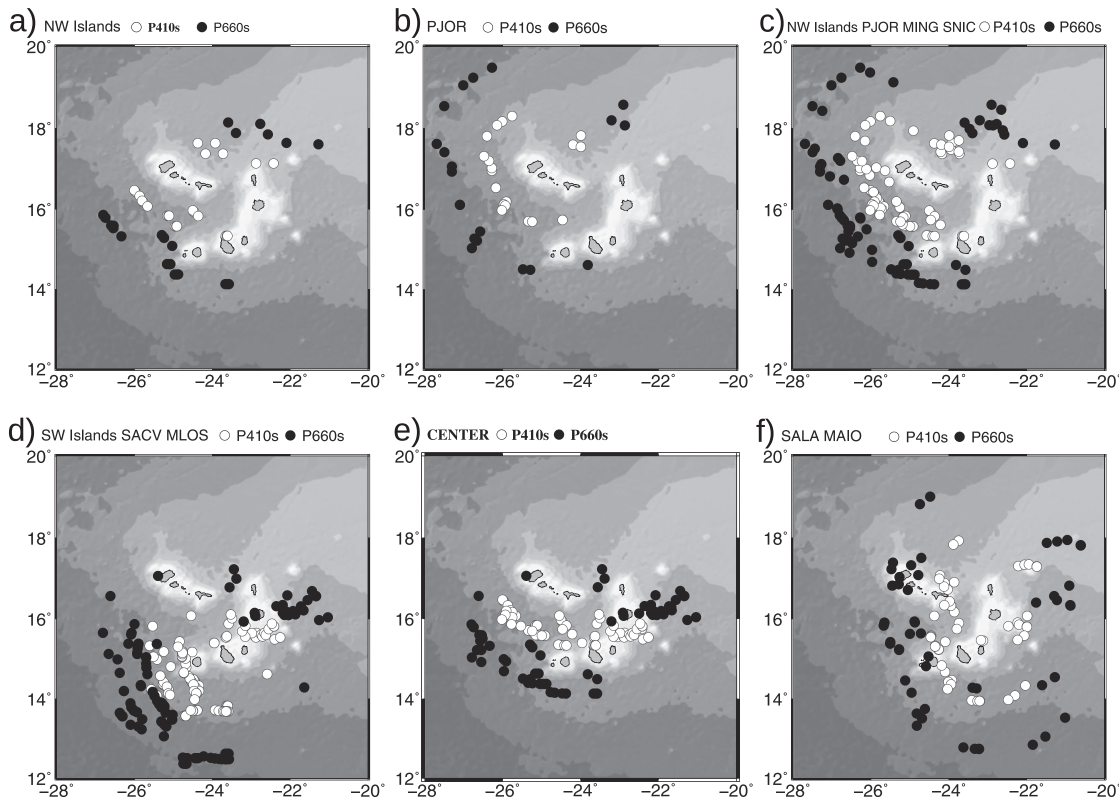

Fig. 4. Piercing points of the Ps converted phases at 410-km (open circles) and 660-km (filled circles depths); a,b,c,d,e,f correspond to Figs. 2 and 3.

continents (Chevrot et al., 1999). The delays of ~3 s indicate that the waves in the upper mantle over the 410-km discontinuity are slow relative to the standard. Similar delays are observed in peripheral regions of Iceland (Du et al., 2006). Piercing points for this set of PRFs are located mostly west of the islands (Fig. 4b). Apparently, west of the islands the structure of the transition zone is nearly normal.

The stack of PRFs for all stations on the north-western islands (Fig. 3c) contains in the time interval from 40 s to 75 s the arrivals that are present in (a) and (b). The M-shaped phase at a time of 53.4 s is preceded by the P410s phase which arrives several seconds earlier (~47.5 s). The times of these two phases can be distorted by interference, but they are close to those in (a) and (b). The P660s phase is outside the interference zone, where it can be easily distorted, but its time (69.6 s) is 1 s less than in (b). The separation between P410s and P660s is 22.1 s. That is 1.8 s less than the standard value. Time anomalies in a range of a fraction of a second can be easily explained by measurement errors (Chevrot et al., 1999), but the anomaly of 1.8 s is too large for this. The piercing points surround the north-western islands; many piercing points are located south and north-east of the islands (Fig. 4c).

In the PRFs from all stations on the south-western islands (Fig. 3d), only an arrival at 45.6 s is detected with confidence in the transition zone window. Most piercing points are located south-west of the south-western islands (Fig. 4d). The reduced delay of P410s relative to IASP91 (1.6 s versus 3.2 s at PJOR) means that the upper-mantle velocities are higher or the 410-km discontinuity is relatively shallow south-west of the Cape Verde archipelago. However, an uplift of the 410-km discontinuity relative to the normal depth at PJOR in a hotspot region is unlikely, and this leaves the relatively high velocities as a likely possibility.

The stack in Fig. 3e differs from the others: PRFs from different stations in this stack sample the same region in the transition zone. This is achieved by using PRFs of all stations on north-western islands for southern events and of all stations on the south-western islands for northern events. Piercing points of this group (Fig. 4e) provide the best sampling of the transition zone under the archipelago. The observed wave field in the transition zone window looks similar to that in Fig. 3c with the M-shaped, P410s and P660s phases. The separation between P410s at 48.5 s and P660s at 68.8 s is 20.3 s, 3.6 s less than the standard time of 23.9 s.

Finally, the stack in Fig. 3f is calculated for PRFs of stations SALA and MAIO on the eastern islands. These data provide good sampling of the transition zone of the Cape-Verde Rise (Fig. 4f). The wave field in Fig. 3f contains P410s and P660s at 46.5 s and 67.4 s with a separation of 20.9 s or 3.0 s less than the standard time. The time of the P660s phase is 3.2 s less that at PJOR which cannot be explained by measurement errors. This is, at least partly, the effect of an uplift of the 660-km discontinuity: 1 s in time is equivalent to ~10 km in depth of the discontinuity.

3. S receiver functions

In S receiver functions (SRFs) the Sp converted phases do not interfere with multiple reflections. In the SRF technique (Farra and Vinnik, 2000) the record of the S wave train is decomposed into Q and L components. For the sketch of the coordinate system see Vinnik et al. (2010). The Q axis is parallel to the principal S-wave particle-motion direction in the wave propagation plane. The L axis is normal to Q in the same plane. The L axis is not disturbed by the S wave motion and, for this reason, is optimal for detecting S-to-P converted phases. The L components of a number of seismic events are equalized by deconvolution. With the adopted sign convention, positive or negative polarity of Sp phase in the L component corresponds to a discontinuity with the lower or higher S velocity at the lower side of the discontinuity. To suppress noise, the deconvolved L components of a number of SRFs are stacked with weights. To account for the difference in slowness between S and Sp phases in the same recording, the SRFs are stacked with move-out time corrections. The corrections are calculated as product of the difference in slowness between the Sp phase and S (differential slowness) and the difference between the epicentral distance of the seismic event and the reference distance. The details of the processing procedure can be found elsewhere (e.g., Silveira et al., 2010; Vinnik et al., 2010).

To construct SRFs with the optimum signal/noise ratio, the records were low-pass filtered with the corner period of 9 s. Sometimes, to maximize the signal/noise ratio in the stack the individual SRFs were combined into groups of two or more stations. The stack of 135 receiver functions from stations SACV, MLOS, SALA and MAIO (Fig. 5a) is calculated for all available good quality recordings in the epicentral distance interval from 65° to 89°. The stack contains a clear S410p phase at a time of −59.8 s. The time of IASP91 model for this phase is −56.1 s (Vinnik et al., 2010), which means that the signal arrives 3.7 s earlier than predicted by the model. The phase, equivalent to the M-shaped phase in Fig. 3, should be recorded in front of S410p with the same amplitude and opposite polarity, but it is not observed. Piercing points of the S410p phase are scattered in a large region outside the Cape Verde Rise (Fig. 5b).

4. Simultaneous inversion of PRFs and SRFs

The simultaneous inversion of PRFs and SRFs was previously applied in several regions, including the Azores (Silveira et al., 2010). The technique was described in detail by Kiselev et al. (2008). We assume that the Earth in the vicinity of the station is laterally homogeneous and isotropic. A search for the optimum models is conducted by using iterative algorithm similar to Simulated Annealing (Mosegaard and Vestergaard, 1991). The procedure is repeated for 4 randomly selected starting points in the model space. For each starting point 10^5 models are tested which is sufficient for the trial models to converge. We divide the model space into cells and present results of the search by a number of hits (color code) in each cell for the last several thousand models. A similar statistics is obtained for the data space. The trial model consists of 9 layers. At a depth of 300 km the velocities are forced to merge with IASP91 velocities.

The synthetics are calculated by using the Thomson–Haskell matrix formalism (Haskell, 1962) for plane waves and plane layers, with Earth flattening transformation (Biswas, 1972). The model is defined by velocities Vp, Vs, thickness and density of each layer. Density is derived from Vp by using Birch's law (Birch, 1961). To reduce the spread of the velocity profiles we invert jointly the receiver functions and teleseismic travel time residuals. The residuals relative to IASP91 can be inferred from the residuals of P410s and P660s. If the time separation between P660s and P410s is close to normal, the average of the residuals of P410s and P660s can be attributed to the Earth's medium above the 410-km discontinuity. This average can be interpreted as the difference between the teleseismic residuals of the S and P waves. The profiles presented in Figs. 6–8 are obtained by assuming that the teleseismic P and S residuals are 1 s and 3 s respectively, and these residuals are accumulated in a depth range of the inversion (300 km). The equivalent residuals of the Ps phases from the transition-zone discontinuities are 2 s, consistent with the data in Fig. 3. For comparison similar profiles with the residuals of 1 s and 4 s are shown in Supplementary material.

The assumption of lateral homogeneity is easily violated in complicated geological structures. To minimize the effects of lateral heterogeneity, we stack receiver functions in wide azimuthal sectors (Figs. 4 and 5b) and combine the receiver functions of neighboring stations. Moreover, we interpret only stable details which are present in the velocity profiles of different stations. The main features of the profiles for station SALA (the eastern islands) (Fig. 6) are: the large discontinuity at a depth of ~10 km, labeled *a*; the underlying layer ~10 km thick with the S velocity of ~3.8 km/s and elevated Vp/Vs ratio (~1.9), labeled *b*; the mantle lid with the S velocity of ~4.1 km/s between the depths of ~20 km and ~65 km, labeled *c* and the underlying layer with a reduced S velocity (~3.8 km/s). These numbers correspond to the medians, whereas the actual values are spread around the medians. The synthetic PRFs and SRFs are close to the actual PRFs and SRFs, and the resulting travel-time residuals for the P and S waves are close to 1 s and 3 s.

The same features are present in the profiles for stations MING and SNIC on the north-western islands (Fig. 7), although there are changes in the parameters: S velocity in the layer *b* is 4.1 km/s instead of 3.8 km/s, the Vp/Vs velocity ratio in this layer is ~2.0 instead of 1.9, and the bottom of this layer is at a depth of ~30 km, instead of 20 km. S velocity in the layer *c* is ~4.2 km/s instead of 4.1 and the upper boundary of the low S-velocity layer is at a depth of ~70 km instead of 65 km. In the profiles for stations SACV and MLOS on the south-

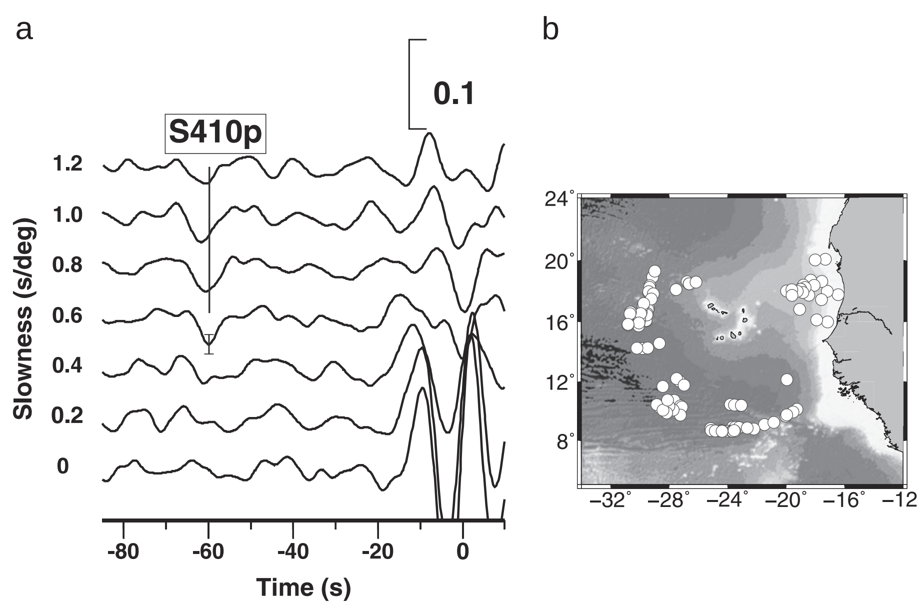

Fig. 5. Stacked SRFs of stations SACV, MLOS, SALA and MAIO (a) and the related piercing points of S410p at a depth of 410 km (b). Move-out corrections for stacking are obtained as product of differential slowness and differential distance. Each trace corresponds to differential slowness shown on the left-hand side. The arrival of S410p phase is marked by $\pm 2\,\sigma$ error bar.

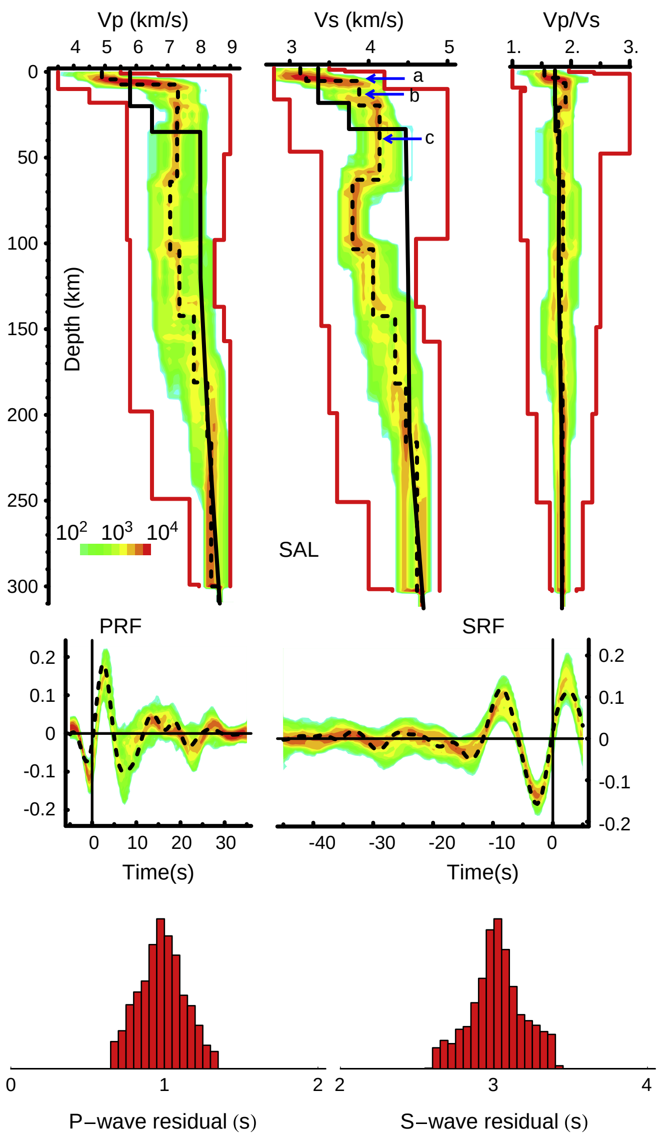

Fig. 6. Simultaneous inversion of PRFs and SRFs from station SALA. Histograms of Vp, Vs and Vp/Vs are shown by color code (upper row). Dash lines are for medians; black solid lines are for IASP91 velocities and their ratio. Labels *a*, *b* and are for the fossil Moho, magmatic underplate and the upper-mantle lid. Middle — histograms of the synthetic PRFs and SRFs, shown by the same color code as the models; dash lines are for the actual PRF and SRF. Bottom — histograms of the travel time residuals of the P and S waves for the models in the upper row. (For interpretation of the references to color in this figure legend, the reader is referred to the web version of this article.)

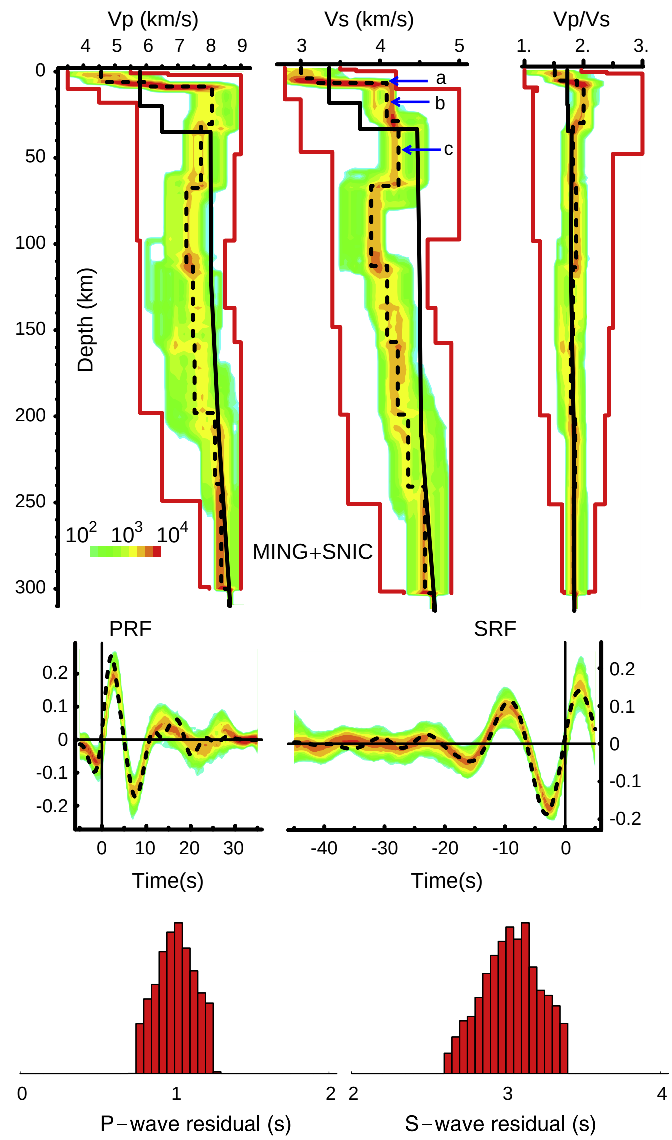

Fig. 7. The same as in Fig. 6 but for stations MING and SNIC.

western islands (Fig. 8) Vp and Vp/Vs ratio in the layer *b* are upward biased, but otherwise the structure is similar to those in Figs. 6 and 7.

The profiles for the residuals of 1 s and 4 s (Figs. 2S–4S of Supplementary materials) are broadly similar to those in Figs. 6–8. A high (relative to the standard 1.8) Vp/Vs velocity ratio in the mantle low-S-velocity zone is a notable detail of the profiles in Figs. 2S–4S.

5. Discussion and conclusions

5.1. Crust and upper mantle

The velocity models in Figs. 6–8 contain a strong boundary *a* at a depth of ~10 km and an underlying layer *b* 10–20 km thick. The Vs and Vp/Vs values in the layer *b* in the profiles for stations SALA and MING + SNIC (~3.9 km/s and ~1.9) are consistent with the data for gabbronorite–troctolite (Christensen, 1996): 3.93 ± 0.12 km/s and 1.86 ± 0.05, respectively. Therefore, in our interpretation, this layer belongs to the crust. As a result, the thickness of the crust (20–30 km) is at least three times the thickness of the normal oceanic crust and is close to other estimates for regions directly above the central rising cores of mantle plumes (20.1 km, White et al., 1992). We interpret the boundary *a* and the underlying layer *b* as the fossil Moho, inherited from the pre-hotspot era, and the magmatic underplate, associated with the plume.

Pim et al. (2008) find in their wide-angle reflection data no evidence for magmatic underplating or a reheating of the upper mantle and a related reduction of the mantle velocity beneath the Cape Verde archipelago. This problem might arise because the difference in P-wave velocities between the crustal layer *b* and the upper-mantle layer *c* is small. In our data layer *b* differs from *c* mainly by the Vp/Vs ratio. Density of gabbro is ~3 g/cm^3 versus 3.3 g/cm^3 for dunite (Christensen, 1996). With a thickness of 10 km the layer *b* may compensate the load of an underwater swell 2 km high. Our data for the crust beneath the Cape Verde islands are fairly similar to those obtained with a similar method for the Azores (Silveira et al., 2010). Indications of underplating are known for other oceanic islands (e.g., Leahy and Park, 2005). Magmatic underplating may support the Cape Verde swell, but we cannot confirm this by gravity modeling, because of a large uncertainty in the required parameters.

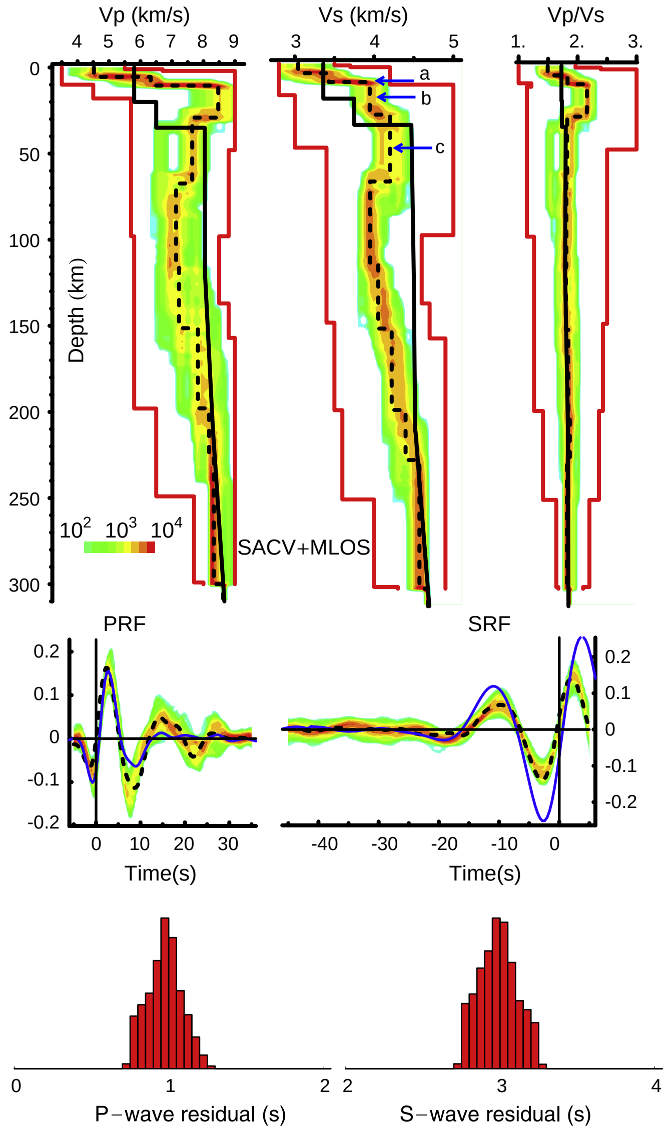

Fig. 8. The same as in Fig. 6 but for stations SACV and MLOS. The synthetic PRFs and SRFs for the model from Lodge and Helffrich (2006) are shown by blue lines. (For interpretation of the references to color in this figure legend, the reader is referred to the web version of this article.)

Like under the Azores, the upper mantle beneath the Cape Verde islands contains the high-velocity lid (layer *c* in Figs. 6–8) and the underlying low S-velocity layer. Qualitatively similar structures are found in a number of oceanic regions (for references see Silveira et al., 2010). This layer is usually interpreted as a residuum formed through basaltic melt extraction (e.g., Gaherty et al., 1996). Beneath the Azores, the S velocity in the lid is ~4.4 km/s, and the Vp/Vs ratio is reduced relative to the normal 1.8 (Silveira et al., 2010). By comparison, the S velocity in the lid beneath the Cape Verde islands (~4.2 km/s) is 5% lower, and the Vp/Vs anomaly is missing. We tentatively relate this difference to the Mid-Atlantic ridge location of the Azores and the mid-plate location of the Cape Verde islands. The S-wave velocity reduction in the low-velocity layer beneath the Cape Verde archipelago and the Azores is 13–15% relative to IASP91 model.

Our uppermost-mantle models are very different from those previously obtained for this region from PRFs by Lodge and Helffrich (2006), furthermore LH: our S velocity is much lower (4.2 km/s versus 4.8 km/s) and there are no indications of extremely low density (2.74 g/cm^3 in LH model versus the standard 3.3 g/cm^3). In comparison with our data, LH models are obtained at a shorter-period (~2 s) range. The low density is invoked in order to reduce the theoretical amplitudes of the multiple reflections from the crust/mantle boundary which are absent in the actual PRFs obtained by LH. This discrepancy may have other reasons. For instance, the reflected phases cannot be observed if the width of the discontinuity is around a quarter of the wavelength or more. For transmitted Ps phases this threshold is roughly 3 times the threshold for reflected phases. If the S-wave period is 2 s, S-wave velocity is 4 km/s and a width of the discontinuity is 3–4 km versus wave-length of 8 km, this discontinuity may produce a large Ps phase and at the same time be transparent for reflected phases, as in the LH data. This, rather than the very low density, is a consistent explanation for incompatibility of the short-period transmitted and reflected phases. The problem of sharpness of the discontinuity is less significant at the longer periods of our study. Another possible reason for the apparent incompatibility of the transmitted and reflected phases is a destructive interference between the multiple reflections from the crust–mantle boundary and the Ps phase from the bottom of the mantle high-velocity lid.

The synthetic receiver functions calculated for LH model differ from our receiver functions of stations MLOS + SACV (Fig. 8). The LH model is obtained only for station SACV, but in our combined data set of SACV + MLOS the data from SACV are strongly dominant. In the PRFs a substantial discrepancy is present in the time interval from 6 to 10 s. This interval contains those seismic phases that are affected by the low density in the LH model. A dramatic disagreement is found between the synthetics and the actual SRFs. Note that the LH model is based only on PRFs, and no wonder that the effect of its non-uniqueness is so large in the SRFs. Separate inversions of both PRFs and SRFs are non-unique, but the non-uniqueness is reduced by the simultaneous inversion in our approach (Vinnik et al., 2004).

To finish the discussion of the low density in the LH model, we note that the material with the ultra-mafic velocity (Vs = 4.8 km/s) and felsic density proposed by LH is very exotic. LH describes this rock as depleted. However, from petrology the fertile mantle has only a 2.5% higher density than the depleted one (O'Hara, 1975), rather than 20% reported by LH. A more realistic density deficit of 2.5% is too small to be inferred directly from seismic amplitudes as attempted by LH.

5.2. Mantle transition zone

Our analysis demonstrates that the separation in time between the P660s and P410s phases beneath the Cape Verde islands is reduced by up to 3.6 s relative to IASP91. The corresponding effect in the thickness of the transition zone is ~30 km. This is a joint effect of uplift of the 660-km discontinuity and depression of the 410-km discontinuity. The times of the P660s phase in the best data are 68.8 s and 67.4 s (Figs. 3e,f), close to 67.9 s in IASP91. For the standard depth of 660 km they should be ~2 s larger, owing to the low velocities in the upper mantle. The discrepancy can be eliminated by moving the 660-km discontinuity to a depth of ~640 km. This is an important observation, because thinning of the transition zone beneath hotspots is usually caused only by depression of the 410-km discontinuity (Deuss, 2007; Du et al., 2006).

The 660-km discontinuity is a combined effect of the post-spinel phase transition with a negative Clapeyron slope of −2.8 MPa/K and the post-majorite transition with a positive Clapeyron slope of 1.3 MPa/K (Hirose, 2002). At a temperature, which can be expected in high-temperature plumes (above 1700–1800 °C), pressure of the combined transition in pyrolite is practically temperature-independent or the pressure–temperature slope is positive (Hirose, 2002). In other words, the depth of the 660-km discontinuity is insensitive to temperature or it is increased by high temperature in such a model. Our observation of the uplift of the 660-km discontinuity contradicts this. If the post-spinel transition is dominant and its pressure-temperature slope is −2.8 MPa/K, the corresponding rate of change of depth of the 660-km discontinuity is −0.07 km/K, and the uplift of 20 km corresponds to a temperature anomaly of +300 K. The negative pressure–temperature slope of the 660-km discontinuity implies that the discontinuity may resist passage of the plume (e.g., Solheim and Peltier, 1994). This is consistent with tomographic images of a few plumes, including the Cape Verde plume (Nolet et al., 2006). Davaille et al. (2005) speculated that the plume may be stopped below/by the transition zone.

Our estimates of the transition zone thickness are very different from the standard width of 250 km, reported by Helffrich et al. (2010). The periods used in the data of Helffrich et al. (2010) (Fig. 9) are somewhat shorter than in our study. Shorter periods may facilitate more accurate estimates of time, but this advantage is only realized when the signal/noise ratio is sufficient, which unfortunately is not the case. We consider the result robust, if the detected seismic phase has a high signal/noise amplitude ratio (at least 3) as well as a specific slowness and waveform. However, the only reason for interpreting the phase in Fig. 9 by Helffrich et al. (2010) as P660s is its appearance in a suitable time interval (near 70 s). In a range between −3° and 0° its amplitude is similar to the noise. At the larger distances its motion is preceded and followed by large oscillations of opposite polarity, which are indicative of interference pattern. Note that the standard differential time between P660s and P410s is 24 s, but in Fig. 9 it reaches 26 s, which implies not thinning but thickening of the transition zone by 20 km.

In our data the S410p phase arrives 3.7 s earlier than predicted by IASP91 model. Qualitatively similar residuals were observed in California (Vinnik et al., 2010) and in the vicinities of the Azores (Silveira et al., 2010). The residual of 2.0 s could be explained either by the Vp/Vs ratio of 1.9 versus ~1.8 in IASP91 in the upper mantle layer 125 km thick or by a depression of the 410-km discontinuity of 15 km or by both effects but of smaller magnitudes (Vinnik et al., 2010). In our case the residual is much larger, as well as the required anomalies of Vp/Vs and depth of the 410-km discontinuity. The region sampled by S410p is very large, because the related first Fresnel zone is elliptic with a half-length of the axis of 900 km in the wave propagation plane (Silveira et al., 2010). A deep depression on the 410-km discontinuity in this region is unlikely, and then the elevated Vp/Vs ratio seems to be a viable alternative. The actual Vp/Vs ratio in the upper mantle may be larger than in our models in Figs. 6–8.

The M-shaped phase in the PRFs is an important finding. This phase is very similar to the phase observed in the Azores region (Fig. 10), but in our data it arrives ~1 s later. The synthetic PRF for this phase in Silveira et al. (2010) was computed for the model with a low S-wave velocity layer between 460-km and 500-km depths (Fig. 10). To fit the wave-train observed in our region, the low-velocity layer in this model should be shifted downward by ~10 km. The model is not unique, but the depth and the S-velocity contrast of the negative discontinuity at the top of the low-velocity layer are constrained by the time and amplitude of the M-shaped phase. This phase is observed in those PRF stacks which provide the highest concentration of the piercing points in the mantle beneath the Cape Verde archipelago. Accordingly, the related structure in the transition zone is present only under the islands and thus is closely related to the recent volcanism. A similar conclusion with respect to the Azores has been made by Silveira et al. (2010). Earlier, the low-velocity layer in the upper transition zone has been found in the SRFs for a few other hotspots (Vinnik and Farra, 2006). Keshav et al. (2011) reported an abrupt drop in the solidus temperature of carbonated mantle in a pressure range corresponding to this low-velocity layer. Indication of a layered structure in the same depth range has been found in PRFs for the Eifel plume (Budweg et al., 2006).

The systematic observations of the plume-related low velocities in the upper transition zone may be relevant to observations of the 520-km discontinuity. At a depth of ~520 km wadsleyite transforms to ringwoodite, but the related velocity increase at this transition in pyrolite is by an order of magnitude less than at the 410-km and 660-km discontinuities and, for this reason, the reflected and converted phases from this discontinuity are practically unobservable. However, there are reports on observations of a discontinuity near this depth, especially in the data on SS precursors (e.g., Deuss and Woodhouse, 2001; Flanagan and Shearer, 1998; Gu et al., 1998) and P wave recordings (e.g., Ryberg et al., 1997). The 520-km discontinuity is found in some regions, but it is absent in the others. In this respect it differs from the global 410-km and 660-km discontinuities. Revenaugh and Jordan (1991) argued that the large 520-km discontinuity in seismic data is related to garnet/post-garnet transformation. Gu et al. (1998) discussed a possibility of very deep continental roots extending into the TZ. Deuss and Woodhouse (2001) reported splitting of the 520-km discontinuity into two discontinuities, whereas Bock (1994) denied evidence for the 520-km discontinuity in precursors to SS.

Our observations suggest that the 520-km discontinuity may be the base of the low velocity layer in the upper transition zone: the related seismic signals are comparable in amplitude with those from the 410-km and 660-km discontinuities, its depth is close to 520 km, and its presence varies on a regional scale.

Acknowledgments

This study was funded by CV-PLUME project (Ref. PTDC/CTE-GIN/64330/2006) and by COBO project GDSS, GFZ-Potsdam. It was partially supported by Pest-OE/CTE/LA0019/2011 — IDL. The instruments for the 2009 deployment were provided by the Geophysical Instrument Pool Potsdam. We thank IRIS DMC for recordings of the permanent station SACV and of the temporary network YW-Cape Verde Mantle Structure. The authors appreciate discussion with Sergio Speziale and helpful comments of two reviewers. L. Vinnik and S. Kiselev were partially supported by RFBR grant 10-05-00879.

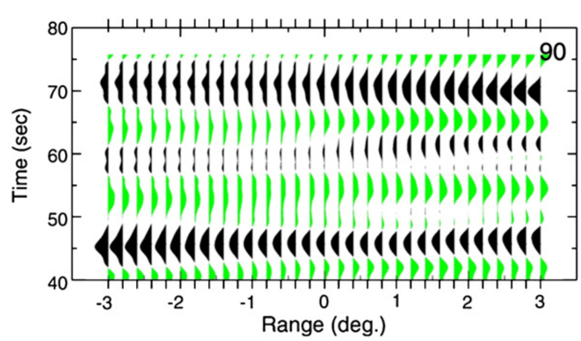

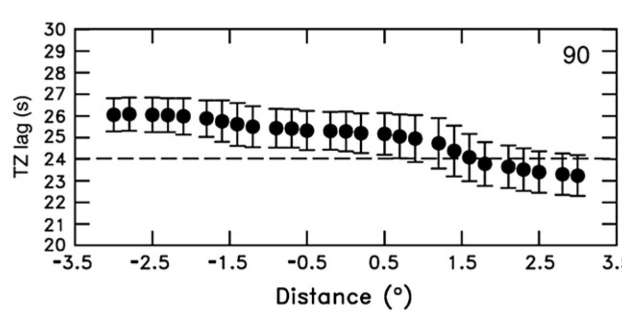

Fig. 9. PRF transect along azimuth of 90° (left-hand side) and the related time lag between 410 and 660 peaks (right-hand side), adopted from Fig. 4 of Helffrich et al. (2010). Origin of the distance scale is at 24°W.

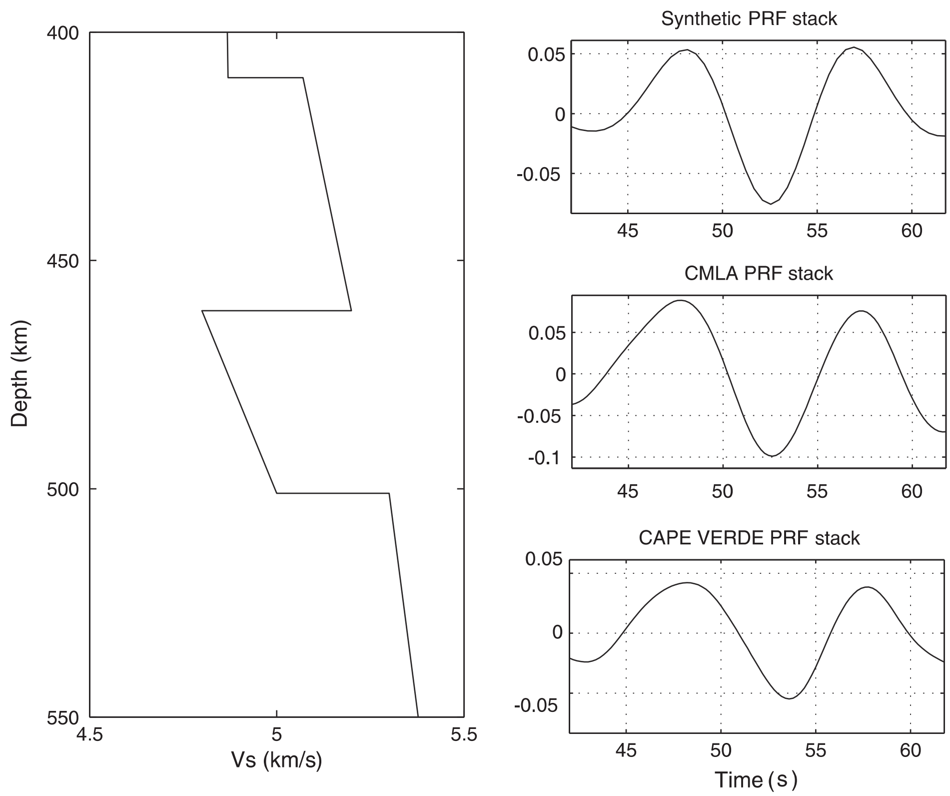

Fig. 10. S velocity profile of the transition zone beneath the Azores (left-hand side). The related synthetic Ps phase, the observed Ps phases from station CMLA on the Azores and from Fig. 3e are shown on the right-hand side. The data for the Azores are adopted from Silveira et al. (2010). Note the striking similarity between the observed Ps phases on the Azores and Cape Verde islands.

Appendix A. Supplementary data

Supplementary data to this article can be found online at doi:10.1016/j.epsl.2011.12.017.

References

Anderson, D.L., 2010. Hawaii, boundary layers and ambient mantle—geophysical constraints. J. Petrol. 52 (7–8), 1547–1577. doi:10.1093/petrology/egq068.

Birch, F., 1961. The velocity of compressional waves in rocks to 10 kilobars. Part 2. J. Geophys. Res. 66, 2199–2224.

Biswas, N.N., 1972. Earth-flattening procedure for the propagation of Rayleigh waves. Pure Appl. Geophys. 96, 61–74.

Bock, G., 1994. Synthetic seismogram images of upper mantle structure: no evidence for a 520-km discontinuity. J. Geophys. Res. 99, 15843–15851.

Budweg, M., Bock, G., Weber, M., 2006. The Eifel Plume-imaged with converted seismic waves. Geophys. J. Int. 166, 579–589.

Chevrot, S., Vinnik, L., Montagner, J.-P., 1999. Global scale analysis of the mantle Pds phases. J. Geophys. Res. 104B, 20,203–20,219.

Christensen, N.I., 1996. Poisson's ratio and crustal seismology. J. Geophys. Res. 101, 3139–3156.

Courtillot, V., Davaille, A., Besse, J., Stock, J., 2003. Three distinct types of hotspots in the Earth's mantle. Earth Planet. Sci. Lett. 205 (3–4), 295–308.

Courtney, R.C., White, R.S., 1986. Anomalous heat flow across the Cape Verde Rise: evidence for a thermal plume in the Earth's mantle. J. R. Astron. Soc. 87, 815–869.

Davaille, A., Stutzmann, E., Silveira, G., Besse, J., Courtillot, V., 2005. Convective patterns under the Indo-Atlantic "box". Earth Planet. Sci. Lett. 239 (3–4), 233–252.

Deuss, A., 2007. Seismic observations of transition-zone discontinuities beneath hotspot locations. In: Foulger, G.R., Jurdy, D.M. (Eds.), Plates, Plumes, and Planetary Processes: Geological Society of America, Special Papers, 430, pp. 121–131.

Deuss, A., Woodhouse, J., 2001. Seismic observations of splitting of the mid-transition zone discontinuity in Earth's mantle. Science 294 (5541), 354–357.

Doglioni, C., Green, D., Mongelli, F., 2005. On the shallow origin of 'hotspots' and the westward drift of the lithosphere. In: Foulger, G.R., Natland, J.H., Presnall, D.C., Anderson, D.L. (Eds.), Plates, Plumes, and Paradigms: Geological Society of America, Special Papers, 388, pp. 733–749.

Du, Z., Vinnik, L.P., Foulger, G.R., 2006. Evidence from P-to-S mantle converted waves for a flat 660-km discontinuity beneath Iceland. Earth Planet. Sci. Lett. 241, 271–280.

Farra, V., Vinnik, L., 2000. Upper mantle stratification by P and S receiver functions. Geophys. J. Int. 141, 699–712.

Flanagan, M.P., Shearer, P.M., 1998. Global mapping of topography of transition zone velocity discontinuities by stacking SS precursors. J. Geophys. Res. 103, 2673–2692.

Forte, A.M., Quere, S., Moucha, R., Simmons, N.A., Grand, S.P., Mitrovica, J.X., Rowly, D.B., 2010. Joint seismic–geodynamic-mineral physical modeling of African geodynamics: a reconciliation of deep-mantle convection with surface geophysical constraints. Earth Planet. Sci. Lett. 295 (3–4), 329–341.

Gaherty, J.B., Jordan, T.H., Gee, L.S., 1996. Seismic structure of the upper mantle in a central Pacific corridor. J. Geophys. Res. 101 (B10), 22291–22309. doi:10.1029/96JB01882.

Gripp, A.E., Gordon, R.G., 2002. Young tracks of hotspots and current plate velocities. Geophys. J. Int. 150, 321–361. doi:10.1046/j.1365-246X.2002.01627.x.

Gu, Y.J., Dziewonski, A.M., Agee, C.B., 1998. Global de-correlation of the topography of transition zone discontinuities. Earth Planet. Sci. Lett. 157, 57–67.

Haskell, N.A., 1962. Crustal reflection of plane P and SV waves. J. Geophys. Res. 67, 4751–4767.

Helffrich, G., Faria, B., Fonseca, J.F.B.D., Lodge, A., Kaneshima, S., 2010. Transition zone structure under a stationary hot spot: Cape Verde. Earth Planet. Sci. Lett. 289 (1–2), 156–161.

Hirose, K., 2002. Phase transitions in pyrolitic mantle around 670-km depth: implications for upwelling of plumes from the lower mantle. J. Geophys. Res. 107 (B4), 2078. doi:10.1029/2001JB000597.

Holm, P.M., Grandvuinet, T., Friis, J., Wilson, J.R., Barker, A.K., Plesner, S., 2008. An ^{40}Ar–^{39}Ar study of the Cape Verde hot spot: temporal evolution in a semistationary plate environment. J. Geophys. Res. 113, B08201. doi:10.1029/2007/JB005339.

Kennett, B., Engdahl, E.R., 1991. Travel times for global earthquake location and phase identification. Geophys. J. Int. 105, 429–465.

Keshav, S., Gudfinnsson, G.H., Presnall, D.C., 2011. Melting phase relations of simplified carbonated peridotite at 12–26 GPa in the systems CaO–MgO–SiO_2–CO_2 and CaO–MgO–Al_2O_3–SiO_2–CO_2: highly calcic magmas in the transition zone of the Earth. J. Petrol. 52, 2265–2291.

Kiselev, S., Vinnik, L., Oreshin, S., Gupta, S., Rai, S.S., Singh, A., Kumar, M.R., Mohan, G., 2008. Lithosphere of the Dharwar craton by joint inversion of P and S receiver functions. Geophys. J. Int. 173, 1106–1118. doi:10.1111/j1365-246X.2008.03777.x.

Leahy, G.M., Park, J., 2005. Hunting for oceanic island Moho. Geophys. J. Int. 160 (3), 1020–1026.

Lodge, A., Helffrich, G., 2006. Depleted swell root beneath the Cape Verde Islands. Geology 36 (6), 449–452. doi:10.1130/G22030.

Monnereau, M., Casenave, A., 2000. Depth and geoid anomalies over oceanic hotspot swells: a global survey. J. Geophys. Res. 95, 15429–15438.

Montelli, R., Nolet, G., Dahlen, F.A., Masters, G., 2006. A catalogue of deep mantle plumes: new results from finite-frequency tomography. Geochem. Geophys. Geosyst. 7 (Q11007), 69. doi:10.1029/2006GC001248.

Morgan, W.J., 1971. Convection plumes in the lower mantle. Nature 230, 42–43.
Mosegaard, K., Vestergaard, P.D., 1991. A simulated annealing approach to seismic model optimization with sparse prior information. Geophys. Prospect. 39, 599–611.
Nolet, G., Karato, S.-I., Montelli, R., 2006. Plume fluxrs from seismic tomography. Earth Planet. Sci. Lett. 248 (3–4), 685–699.
O'Hara, M.J., 1975. Is there an Icelandic plume? Nature 253, 708–710.
Pim, J., Peirce, C., Watts, A.B., Grevemeyer, I., Krabbenhoeft, A., 2008. Crustal structure and origin of the Cape Verde Rise. Earth Planet. Sci. Lett. 272 (1–2), 422–428.
Revenaugh, J., Jordan, T., 1991. Mantle layering from ScS reverberatios 1. Waveform inversion of zeroth-order reverberations. J. Geophys. Res. 96 (B12), 19749–19762.
Ritsema, J., Allen, R.M., 2003. The elusive mantle plumes. Earth Planet. Sci. Lett. 207, 1–12. doi:10.1016/S0012-821X(02)01093-2.
Ryberg, T., Wenzel, F., Egorkin, A.V., Solodilov, L., 1997. Short-period observation of the 520 km discontinuity in northern Eurasia. J. Geophys. Res. 102 (B3), 5413–5422.
Silveira, G., Stutzmann, E., Davaille, A., Montagner, J.-P., Mendes-Victor, L., Sebai, A., 2006. Azores hotspot signature in the upper mantle. J. Volcanol. Geotherm. Res. 156 (1–2), 23–34.
Silveira, G., Vinnik, L., Stutzmann, E., Farra, V., Kiselev, S., Morais, I., 2010. Stratification of the Earth beneath the Azores from P and S receiver functions. Earth Planet. Sci. Lett. 299, 91–103.
Solheim, L.P., Peltier, W.R., 1994. Phase boundary deflections at 660-km depth and episodically layered isochemical convection in the mantle. J. Geophys. Res. 99 (B8), 15861–15875.
Tauzin, B., Debayle, E., Wittlinger, G., 2008. The mantle transition zone as seen by global Pds phases: no clear evidence for a thin transition zone beneath hotspots. J. Geophys. Res. 113, B08309. doi:10.1029/2007/B005364.
Vinnik, L., 1977. Detection of waves converted from P to SV in the mantle. Phys. Earth Planet. Inter. 15, 39–45.
Vinnik, L., Farra, V., 2006. S velocity reversal in the mantle transition zone. Geophys. Res. Lett. 33, L18316. doi:10.1029/2006GL027120.
Vinnik, L.P., Reigber, Ch., Aleshin, I.M., Kosarev, G.L., Kaban, M.K., Oreshin, S.I., Roecker, S.W., 2004. Receiver function tomography of the central Tien Shan. Earth Planet. Sci. Lett. 225 (1–2), 131–146.
Vinnik, L., Ren, Y., Stutzmann, E., Farra, V., Kiselev, S., 2010. Observations of S410p and S350p phases at seismograph stations in California. J. Geophys. Res. 115, B05303. doi:10.1029/2009JB006582.
White, R.S., McKenzie, D., O'Nions, R.K., 1992. Oceanic crustal thickness from seismic measurements and rare earth elements. J. Geophys. Res. 97 (B13), 19,683–19,715.